A model for jumping and bubble waves in the Belousov–Zhabotinsky-aerosol OT system

Vladimir K. Vanag[a] and Irving R. Epstein[b]
Department of Chemistry, MS 015, Brandeis University, Waltham, Massachusetts 02454, USA

(Received 24 July 2009; accepted 26 August 2009; published online 14 September 2009)

We develop a four-variable model, based on the classic Field–Kőrös–Noyes mechanism for the oscillatory Belousov-Zhabotinsky (BZ) reaction, that describes recently discovered jumping waves and bubble waves in the BZ reaction in aerosol OT microemulsion and provides insight into their origins. Contrary to suggestions based on previous models, it appears that these phenomena can arise from interaction between a Turing instability and either excitability or a Hopf instability of the steady state, rather than requiring a wave instability. The model should be useful for studying other patterns in BZ microemulsions as well as the behavior of systems of BZ microdroplets coupled through bromine diffusion. © *2009 American Institute of Physics*. [doi:10.1063/1.3231488]

I. INTRODUCTION

The well-known Belousov-Zhabotinsky (BZ) reaction, in which malonic acid is catalytically oxidized by bromate in acidic medium[1,2] has been described by a number of models, many of which are based on the detailed Field–Kőrös–Noyes (FKN) mechanism[3] or simplifications of it, e.g., the Oregonator model.[4] We have recently proposed further modifications of the Oregonator model in order to describe patterns in the BZ-AOT water-in-oil microemulsion system (AOT is the surfactant, aerosol OT).[5–7] The recent discovery of novel jumping waves (JWs) and bubble waves (BWs) in the BZ-AOT system,[8] as well as the development of a new experimental system, water microdroplets containing the BZ reactants coupled via diffusion of oil-soluble intermediates of the BZ reaction, Br_2 and $BrO_2^{\bullet}$, through oil gaps between droplets,[9] suggest the need for a new model for the BZ reaction. Earlier detailed models (such as FKN) are too cumbersome to describe systems containing large numbers of drops; others (such as the Oregonator) are too simple to account for phenomena like JW. We seek to develop a model of intermediate complexity that is simple enough to allow some degree of analysis, yet retains enough detail to describe the new phenomena (JW and BW) found in experiments.

Our approach is as follows. We first derive a suitable model for the BZ reaction starting from the full FKN model augmented by terms that describe the interaction of the catalyst with light. We simplify the model by a series of approximations in which some concentrations are taken as constant, while others are eliminated through quasiequilibrium or steady state (SS) approximations. In this fashion, we are able to reduce the model to four variables, including one that will be used at the next stage to characterize interactions between droplets in the microemulsion system. After some analysis of the steady state of this model and its stability properties, we add two new variables to describe the messenger species bromine in the surfactant and oil phases of the microemulsion. A further reduction process enables us to obtain a four-variable model for the BZ-AOT system with renormalized diffusion and rate constants to take into account the effects of the microemulsion. We then carry out numerical simulations of JW and BW and analyze our results to gain insight into the origin of these phenomena.

II. MODELING THE BZ REACTION

We start from the FKN model[3]

$$X + Y + H^+ \rightarrow 2P, \quad k_1 = 2 \times 10^6 h \quad (M^{-1}\ s^{-1}), \tag{1}$$

$$Y + A + 2H^+ \rightarrow X + P, \quad k_2 = 2h^2 a \quad (s^{-1}), \tag{2}$$

$$X + X \rightarrow P, \quad k_3 = 3000 \quad (M^{-1}\ s^{-1}), \tag{3}$$

$$X + A + H^+ \rightarrow 2W, \quad k_4 = 42ha \quad (s^{-1}), \tag{4}$$

$$Y + P + H^+ \rightarrow U, \quad k_5 = 5 \times 10^9 h \quad (M^{-1}\ s^{-1}), \tag{5}$$

$$U \rightarrow Y + P + H^+, \quad k_6 = 10 \quad (s^{-1}), \tag{6}$$

$$U + MA \rightarrow Y + BrMA, \quad k_7 = 29m \quad (s^{-1}), \tag{7}$$

$$P + MA \rightarrow BrMA, \quad k_8 = 9.3m \quad (s^{-1}), \tag{8}$$

$$H_2O + W + W \rightarrow X + A + H^+, \quad k_r = 2 \times 10^8 \quad (M^{-1}\ s^{-1}), \tag{9}$$

$$W + C \rightarrow X + Z, \quad k_{red} = 5 \times 10^6 \quad (M^{-1}\ s^{-1}), \tag{10}$$

$$Z + BrMA \rightarrow Y + C, \quad k_9 = k_9' b \quad (s^{-1}), \tag{11}$$

$$Z + MA \rightarrow C, \quad k_{10} = 0.05m \quad (s^{-1}), \tag{12}$$

where the concentrations of protons $h=[H^+]$, bromate $a=[A]$, malonic acid $m=[MA]$, and bromomalonic acid $b=[BrMA]$ are taken as constants, and $x=[X]=[HBrO_2]$, $y=[Y]=[Br^-]$, $p=[P]=[HOBr]$, $w=[W]=[BrO_2^{\bullet}]$, $u=[U]$

[a]Electronic mail: vanag@brandeis.edu.
[b]Electronic mail: epstein@brandeis.edu.

$=[Br_2]$, $c=[C]$ (reduced form of the catalyst), and $z=[Z]$ (oxidized form of the catalyst) are variables.

When the photosensitive $Ru(bpy)_3$ complex is used as the catalyst, we add the additional reactions[10,11]

$$C + h\nu \rightarrow C^*, \quad k(I), \tag{13}$$

$$C^* + \mathrm{BrMA} \rightarrow Z + Y, \quad k_C, \tag{14}$$

$$C^* \rightarrow C, \quad k_d. \tag{15}$$

If we make the SS approximation for the excited state C^*, the corresponding set of ordinary differential equations is

$$dx/dt = -k_1xy + k_2y - 2k_3x^2 - k_4x + k_rw^2 + k_{\mathrm{red}}wc, \tag{16}$$

$$dy/dt = -k_1xy - k_2y - k_5yp + k_6u + k_7u + k_9z + k(I)cb/(b_C + b), \tag{17}$$

$$dz/dt = k_{\mathrm{red}}wc - k_9z - k_{10}z + k(I)cb/(b_C + b), \tag{18}$$

$$dp/dt = 2k_1xy + k_2y + k_3x^2 - k_5yp + k_6u - k_8p, \tag{19}$$

$$du/dt = k_5yp - k_6u - k_7u, \tag{20}$$

$$dw/dt = 2k_4x - 2k_rw^2 - k_{\mathrm{red}}wc, \tag{21}$$

$$dc/dt = -k_{\mathrm{red}}wc + k_9z + k_{10}z - k(I)cb/(b_C + b), \tag{22}$$

where $b_C=k_d/k_C=0.05M$.[10,12]

Experiments on patterns in a one-dimensional (1D) array of coupled BZ droplets[9] imply that inhibitory coupling of the BZ microdroplets through oil-soluble Br_2 dominates, since waves, which require coupling through an activator, were not found. This result allows us to eliminate $BrO_2^{\bullet}$ (w) from the model by making the SS approximation, i.e., setting $dw/dt=0$. From Eq. (21) we have $k_{\mathrm{red}}wc=2k_4x-2k_rw^2$. Substituting this expression into Eqs. (16), (18), and (22) and ignoring k_rw^2 (since $k_{\mathrm{red}}c \gg 2k_rw$ at almost all times during the reaction), we have

$$dx/dt = -k_1xy + k_2y - 2k_3x^2 + k_4x, \tag{23}$$

$$dz/dt = 2k_4x - k_9z - k_{10}z + k(I)c/(b_C/b + 1), \tag{24}$$

$$dc/dt = -2k_4x + k_9z + k_{10}z - k(I)c/(b_C/b + 1). \tag{25}$$

Also, $z+c=c_0$, where c_0 is the total concentration of the catalyst, so we can replace c by c_0-z. The resulting equations have the defect that the autocatalytic term, k_4x in Eq. (23), is not limited by the depletion of the reduced form of the catalyst c. The classic Oregonator model[4] suffers from the same flaw. To resolve this problem, some authors[6,13] modify the autocatalytic term as $k_4xc/(c+c_{\min})$, where $c_{\min}$ is a small constant. This constant can be determined from the condition that the rates of reactions 9 and 10 when $c=c_{\min}$ (when the rate of autocatalysis is a maximum) are approximately equal (note that in most other phases of the reaction $k_{\mathrm{red}}c \gg 2k_rw$) so that

$$k_{\mathrm{red}}c_{\min} = 2k_rw_{\max}, \tag{26}$$

where the maximum concentration of the radical $w_{\max}$ can be found with the aid of the following equation [cf. Eq. (18) when $k(I)=0$]:

$$k_{\mathrm{red}}w_{\max}c_{\min} = k_9c_0 + k_{10}c_0. \tag{27}$$

Equations (26) and (27) give

$$c_{\min}^2 = 2k_r(k_9 + k_{10})c_0/k_{\mathrm{red}}^2. \tag{28}$$

Our next simplification is to eliminate the fast variable p. We set $dp/dt=0$ in Eq. (19) and find the quasistationary p. We note that $k_5yp \gg k_8p$ at nearly all times, since $k_5y_{\mathrm{cr}} \gg k_8$, where $y_{\mathrm{cr}}=k_4/k_1$ (y_{cr} is the critical concentration of the inhibitor bromide below which autocatalytic reactions 4 and 9 start). If so, we can drop the term k_8p from Eq. (19) to give $k_5yp=-2k_1xy-k_2y-k_3x^2-k_6u$. Substituting this result in Eqs. (17) and (20) and taking into account the previous simplifications, we finally have our four-variable model

(A)
$$dx/dt = -k_1xy + k_2y - 2k_3x^2 + k_4x(c_0 - z)/(c_0 - z + c_{\min}), \tag{29}$$

$$dy/dt = -3k_1xy - 2k_2y - k_3x^2 + k_7u + k_9z + k(I)(c_0 - z)/(b_C/b + 1), \tag{30}$$

$$dz/dt = 2k_4x(c_0 - z)/(c_0 - z + c_{\min}) - k_9z - k_{10}z + k(I)(c_0 - z)/(b_C/b + 1), \tag{31}$$

$$du/dt = 2k_1xy + k_2y + k_3x^2 - k_7u. \tag{32}$$

Direct simulations of models (16)–(22) and (29)–(32) give very similar results: the shape, period, and amplitude of oscillations of all variables are nearly the same in both models. The fastest remaining variable is u [$k_7^{-1}=(29m)^{-1}=0.03-1$ s], but it cannot be eliminated through a quasiequilibrium approximation, since u is used in coupling the BZ droplets. Elimination of the other fast variable y results in a reduced system whose behavior differs significantly from that of the original system (16)–(22).

Model (29)–(32), which we designate as model (A), can be reduced to dimensionless form, but the speed of simulation remains almost the same. We therefore work with the dimensional model, where the link between our parameters and the corresponding experimental quantities is clear. Nevertheless for completeness, we present here the dimensionless equations. Introducing new dimensionless variables (similar to the scaling usually employed in the Oregonator model), $x=\bar{x}k_4/(2k_3)$, $y=\bar{y}k_4/k_1$, $z=\bar{z}k_4^2/[k_3(k_9+k_{10})]$, $u=\bar{u}k_4^2/(k_3k_7)$, $t=\tau/(k_{10}+k_9)$, and seven (eight including the light intensity) new parameters $q=2k_2k_3/(k_4k_1)$, $\varepsilon_1=(k_{10}+k_9)/k_4$, $\varepsilon_2=2(k_{10}+k_9)k_3/(k_4k_1)$, $\varepsilon_3=(k_{10}+k_9)/k_7$, $g=k_9/(k_9+k_{10})$, $\varepsilon=c_{\min}/c_0$, $z_m=k_3(k_9+k_{10})c_0/k_4^2$, and $\phi(I)=k(I)c_0(k_3/k_4^2)/(b_C/b+1)$ [note that $\phi(I) \ll 1$, since $k(I)$ is usually in the range of $10^{-7}-10^{-5}$ s^{-1}], model (29)–(32) assumes the form

$$\varepsilon_1 d\bar{x}/d\tau = -\bar{x}\bar{y} + q\bar{y} - \bar{x}^2 + \bar{x}(1 - \bar{z}/z_m)/(1 - \bar{z}/z_m + \varepsilon), \tag{29′}$$

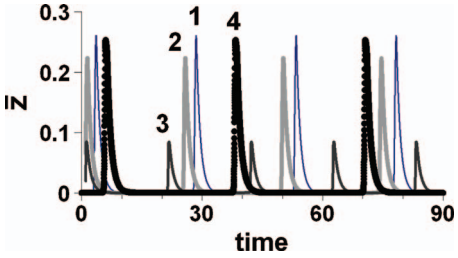

FIG. 1. Comparison of the Oregonator model (curve 1) and model (29′)–(32′) (curves 2–4). Parameters: ε_1=0.054, ε_2=0.001 08, q=0.000 143, and g=0.706, ε_3=(curves 2 and 3) 0.005 86, (4) 0.879, z_m=(2,4) 0.257, (3) 0.0857, ε=(2,4) 0.0233, (3) 0.0404.

$$\varepsilon_2 d\bar{y}/d\tau = -3\bar{x}\bar{y} - 2q\bar{y} - \bar{x}^2/2 + 2\bar{u} + 2g\bar{z} + 2\phi(I)(1-\bar{z}/z_m), \tag{30′}$$

$$d\bar{z}/d\tau = \bar{x}(1-\bar{z}/z_m)/(1-\bar{z}/z_m+\varepsilon) - \bar{z} + \phi(I)(1-\bar{z}/z_m), \tag{31′}$$

$$\varepsilon_3 d\bar{u}/d\tau = \bar{x}\bar{y} + q\bar{y}/2 + \bar{x}^2/4 - \bar{u}. \tag{32′}$$

Note that the Oregonator model,[4] which we refer to as "O," has four parameters, ε_1, ε_2, q, and g,

$$\text{(O)} \quad \varepsilon_1 dx/d\tau = -yx + qy - x^2 + x,$$

$$\varepsilon_2 dy/d\tau = -yx - qy + 2gz,$$

$$dz/d\tau = x - z,$$

while our model (29′)−(32′) has 7 parameters [if $\phi(I)=0$]. Note also, that if we eliminate $\bar{u}$ via a quasiequilibrium for Eq. (32′), $\bar{u}=\bar{x}\bar{y}+q\bar{y}/2+\bar{x}^2/4$, and substitute this expression into Eq. (30′), then Eq. (30′) becomes identical to the second equation of system (O), and the system (29′) and (32′) is nearly the same as (O), to which it reduces at $\varepsilon=0$.

Comparing models (O) and (29′)−(32′) [at $\phi(I)=0$ for simplicity], we see that system (29′)−(32′) has three additional parameters, ε, z_m, and ε_3, and its behavior is strongly dependent on the rate constant k_7 and the concentration c_0, parameters that do not arise in the Oregonator model. We can compare these models at the same set of common parameters ε_1, ε_2, q, and g (see Fig. 1), the values of which are calculated at the typical experimental concentrations $h=0.15M$, $a=0.3M$, and $m=0.6M$, and we assume that $k_9=k_9'b=k_9''m$ with $k_9''=0.12$ s^{-1}. The other parameters of model (29′)–(32′), ε_3, z_m, and ε, are calculated at three different sets of c_0 and k_7, i.e., catalyst and malonic acid concentrations: $c_0=0.003M$ and $k_7=17.4$ s^{-1} (this value of k_7 corresponds to the reaction in the aqueous phase) (curve 2); $c_0=0.001M$ and $k_7=17.4$ s^{-1} (curve 3), and $c_0=0.003M$, $k_7=17.4/150$ s^{-1} (this value of k_7 corresponds to the reaction in the BZ-AOT system, see below) (curve 4). We see in Fig. 1 that at some values of c_0 (=0.003M) and small ε_3 (large k_7) the models give similar behavior with almost the same period and amplitude of oscillation (curves 1 and 2). However, if c_0 is smaller (=0.001M) (curve 3) or ε_3 is larger (small k_7) (curve 4), the difference between the two models is significant.

A. Steady state

The steady state(s) (SS) of system (29)–(32) (model A) at $\phi(I)=0$ can be found by solving numerically the following equations:

$$x_{SS} = \alpha z_{SS}(1 - z_{SS}/c_0 + \varepsilon)/(1 - z_{SS}/c_0), \tag{33}$$

$$x_{SS} = \mu[k_9 + F(z_{SS})]/[k_9 - F(z_{SS})], \tag{34}$$

where $F(z_{SS})=\alpha k_4 - 2k_3\alpha^2 z_{SS}(1-z_{SS}/c_0+\varepsilon)^2/(1-z_{SS}/c_0)^2$, $\mu=k_2/k_1$, and $\alpha=(k_9+k_{10})/(2k_4)$. Then $y_{SS}=k_9 z_{SS}/(k_1 x_{SS}+k_2)$, $u_{SS}=(2k_1 x_{SS} y_{SS}+k_2 y_{SS}+k_3 x_{SS}^2)/k_7$. Model (A) has a single SS, since the right hand side of Eq. (33) is monotonically increasing and that of Eq. (34) is monotonically decreasing for allowable values of z_{SS}, if $k_9 > k_{10}$, which is true. Note that $k_9 > k_{10}$ implies that the stoichiometric factor in Eq. (30′), $g > 0.5$.

When $\phi(I) \neq 0$, the SS of model (A) can be found numerically by solving

$$f_2(z)(k_2 - k_1 x_{SS})/(k_1 x_{SS} + k_2) - 2k_3 x_{SS}^2 + x_{SS} f_1(z) = 0, \tag{35}$$

where

$$x_{SS} = f_3(z)/2f_1(z), \tag{36}$$

where $f_1(z)=k_4(c_0-z)/(c_0-z+c_{min})$, $f_2(z)=k_9 z+k(I)(c_0-z)/(b_C/b+1)$, and $f_3(z)=k_9 z+k_{10}z-k(I)(c_0-z)/(b_C/b+1)$. After finding z_{SS} and x_{SS}, we can find first y_{SS} and then u_{SS} as $y_{SS}=f_2(z_{SS})/(k_1 x_{SS}+k_2)$ and $u_{SS}=(2k_1 x_{SS} y_{SS}+k_2 y_{SS}+k_3 x_{SS}^2)/k_7$.

B. Linear stability analysis of model (A)

Knowing the SS of model (A), we can proceed to analyze its stability. With $\phi(I)=0$, we varied the key parameters of the model, h, a, m, and k_9'', where $k_9=k_9'b=k_9''m$ (k_9'' depends on the initial concentration of Br^- and consequently on the initial b), over broad ranges, though in experiments m is usually confined to values between 0.03 and 1, h between 0.05 and 1, and a between 0.05 and 0.5. The phase diagram is shown in Fig. 2. The onset of Hopf instability (lines 1–6 in Fig. 2) occurs from both sides of the oscillatory region via a canard phenomenon.[14] The boundary between the oscillatory state and the reduced SS (curves 1–3) shifts toward the SS as k_9'' decreases or h increases. The boundary between the oscillatory state and the oxidized SS (curves 4–6) moves toward the SS as k_9'' increases or h decreases.

III. MODELING THE BZ-AOT SYSTEM

To describe the BZ-AOT system, we add two new variables to model (A), Br_2 in the oil phase, u_O, and Br_2 in the surfactant pseudophase, u_S, and we rename the variable u in the aqueous phase as u_W. We normalize the concentrations in the three phases (the aqueous phase with volume fraction φ_W, the oil phase with volume fraction φ_{oil}, and the surfactant phase with volume fraction φ_S, $\varphi_W+\varphi_{oil}+\varphi_S=1$) to the bulk concentrations (subscript b) as $\varphi_W x_W = x_b$, $\varphi_W y_W = y_b$, $\varphi_W z_W = z_b$, $\varphi_W c_{0W} = c_{0b}$, $\varphi_W u_W = u_{Wb}$, $\varphi_S u_S = u_{Sb}$, $\varphi_{oil} u_O = u_{Ob}$. We also add diffusion coefficients for all variables, since we

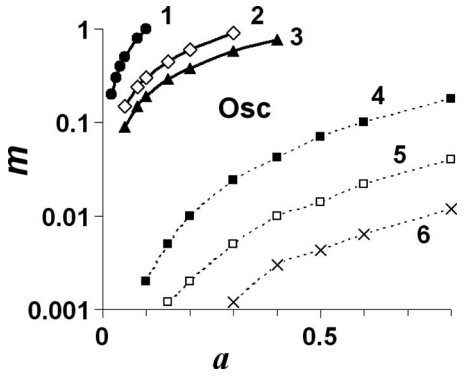

FIG. 2. Phase diagram in the a-m plane for models (29)–(32). All curves correspond to the onset of Hopf instability. Parameters: h =(curves 1 and 3) 0.16, (2, 6) 0.2, (4 and 5) 0.4, k_9''=(1) 0.15, (2, 3) 0.2, (4) 0.06, (5, 6) 0.1. "Osc" denotes the oscillatory region. Curves 1–3 are well fitted by lines $m=C_i\times a$, where $C_i=(i=1)$ 10, (2) 3, (3) 1.92, while curves 4 and 5 are well fitted by lines $m=C_i\times a^n$, where n=2.1–2.3 and $C_i=(i=4)$ 0.306, (5) 0.064, and (6) 0.0207. For curves 1–3, the SS (reduced) is above and to the left of the curves, while for curves 4–6, the SS (oxidized) is below and to the right.

wish now to model the reaction-diffusion system in order to explain JW and BW. The new equations for u_{Wb}, u_{Sb}, and u_{Ob} are

$$du_{Wb}/dt = 2k_1x_by_b/\varphi_W + k_2y_b + k_3x_b^2/\varphi_W - k_7u_{Wb} - k_{f1}u_{Wb} + (\varphi_W/\varphi_S)k_{b1}u_{Sb} + D_d\nabla^2u_{Wb}, \quad (37)$$

$$du_{Sb}/dt = (\varphi_S/\varphi_W)k_{f1}u_{Wb} - k_{b1}u_{Sb} - k_{f2}u_{Sb} + (\varphi_S/\varphi_{\text{oil}})k_{b2}u_{Ob} + D_s\nabla^2u_{Sb}, \quad (38)$$

$$\partial u_{Ob}/\partial t = (\varphi_{\text{oil}}/\varphi_S)k_{f2}u_{Sb} - k_{b2}u_{Ob} + D_u\nabla^2u_{Ob}, \quad (39)$$

where k_{f1} and k_{f2} are the rate constants (s^{-1}) for the transfer of Br_2 from water to the AOT shell (surfactant phase), and from the AOT shell to the oil phase, respectively, and k_{b1} and k_{b2} are the corresponding rate constants for the respective reverse processes. The molecular diffusion coefficient D_u is of order 10^{-5} cm^2/s, while D_d, the diffusion coefficient of a droplet, is 10^{-6}–10^{-7} cm^2/s (depending on the droplet size), and D_s is the diffusion coefficient of Br_2 in the surfactant shell. It is reasonable to take $D_d<D_s<D_u$.

Summing Eq. (37)+$(\varphi_W/\varphi_S)\times$Eq. (38)+$(\varphi_W/\varphi_{\text{oil}})\times$Eq. 39, we have

$$\partial u_b/\partial t = 2k_1x_by_b/\varphi_W + k_2y_b + k_3x_b^2/\varphi_W - k_7'u_b + D_u'\nabla^2u_b, \quad (40)$$

where $u_b=\varphi_W(u_W+u_S+u_O)$, and

$$k_7' = k_7/[1 + k_{f1}/k_{b1} + k_{f1}k_{f2}/(k_{b1}k_{b2})], \quad (41)$$

The effective diffusion coefficient D_u' is determined from the equation

$$D_d\nabla^2u_W + D_s\nabla^2u_S + D_u\nabla^2u_O = D_u'\nabla^2u_b/\varphi_W \quad (42)$$

as

$$D_u' = [D_u + D_sk_{b2}/k_{f2} + D_dk_{b2}/k_{f2}(k_{b1}/k_{f1})]/[1 + k_{b2}/k_{f2} + k_{b1}k_{b2}/(k_{f1}k_{f2})]. \quad (43)$$

Equations (41) and (43) are obtained by assuming that all rate constants k_{f1}, k_{f2}, k_{b1}, and k_{b2} are very large, since the diffusion of Br_2 between phases is rapid at the nanometer distances involved here, and that the following equilibria hold

$$k_{f2}u_S = k_{b2}u_O \quad \text{and} \quad k_{f1}u_W = k_{b1}u_S. \quad (44)$$

Returning in Eq. (40) to the concentrations in the aqueous phase and using the equality $u_W=u_t/[1+k_{f1}/k_{b1}+k_{f1}k_{f2}/(k_{b1}k_{b2})]$ in Eq. (30) (where $u_t=u_W+u_S+u_O$) to replace k_7u_W with $k_7'u_t$, we finally have our model (B) for the BZ-AOT system at $k(I)=0$ (where we omit for simplicity subscripts W for x, y, and z, and subscript t for u)

(B)
$$dx/dt = -k_1xy + k_2y - 2k_3x^2 + k_4x(c_0-z)/(c_0-z+c_{\min}) + D_d\nabla^2x,$$

$$dy/dt = -3k_1xy - 2k_2y - k_3x^2 + k_7'u + k_9z + D_d\nabla^2y,$$

$$dz/dt = 2k_4x(c_0-z)/(c_0-z+c_{\min}) - k_9z - k_{10}z + D_d\nabla^2z,$$

$$\partial u/\partial t = 2k_1xy + k_2y + k_3x^2 - k_7'u + D_u'\nabla^2u.$$

We can estimate the constants k_7' and D_u'. Note that

$$k_{f1}/k_{b1} = P_{B1}/r_{V1}, \quad k_{f2}/k_{b2} = P_{B2}/r_{V2}, \quad (45)$$

where P_{B1} and P_{B2} are the partition coefficients for Br_2 between AOT and water and between oil and AOT, respectively, and $r_{V1}=V_S/V_W=\varphi_S/\varphi_W$, $r_{V2}=V_{\text{oil}}/V_S=\varphi_{\text{oil}}/\varphi_S$, the volume ratios of the corresponding phases. For $\varphi_d=\varphi_W+\varphi_S=0.4$ (i.e., below the percolation threshold), using the relation $\varphi_d\cong 2.5\varphi_W$ [for $\omega=15$ (Ref. 15)], which gives $r_{V1}\cong 1.5$ and $r_{V2}\cong 2.5$, and assuming that $P_{B2}=0.2$ (Ref. 16) and $P_{B1}=100$ (since $P_{B1}P_{B2}=P_{B3}$, where $P_{B3}\cong 20$, the partition coefficient between water and octane[9]), we obtain $k_7'\cong k_7/73$ and $D_u'\cong D_u/14$ for $D_s=D_d=0.01D_u$ and $D_u'\cong D_u$ for $D_s=D_u=100D_d$. The coefficient D_u' should in general be smaller than D_u due to the ability of the AOT-shell (large aggregate of surfactant molecules) to transiently capture Br_2 and thereby slow its diffusion.

In the dimensionless Eqs. (29′)–(32′), k_7 should be replaced by $k_7':u=\bar{u}k_4^2/k_3k_7'$, and $\varepsilon_3=(k_{10}+k_9)/k_7'$. Note that ε_3 becomes almost 100 times larger and the variable $\bar{u}$ is no longer a fast variable. The other constants in the model also require adjustment to take into account the fact that the environment in the water droplets of the BZ-AOT system differs from that in the pure aqueous system. For example, the concentration of protons is much smaller due to protonation of the SO_3^- groups of the AOT molecules.[17]

A. Linear stability analysis of model (B)

Linear stability analysis of system (B) reveals a broad range of parameters in which Turing instability occurs. A typical dispersion curve for Turing instability is shown in

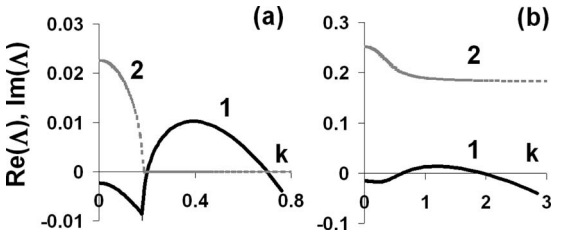

FIG. 3. Dispersion curves for model (B). (a) Turing instability. (b) Wave instability. Curves 1 and 2 are, respectively, $\mathrm{Re}(\Lambda)$ and $\mathrm{Im}(\Lambda)$, where Λ is the eigenvalue of the linearized model (B) with the largest real part. Parameters: (a) $h=0.08$, $a=0.1$, $m=0.5$, $c_0=0.003$, $k_1=2\times10^6 h$, $k_2=2h^2a$, $k_3=3000$, $k_4=42ha$, $k_7'=29m/150$, $k_9=0.12m$, $k_{10}=0.05m$, $c_{\min}$ is calculated from Eq. (28) at $k_r=2\times10^8$ and $k_{\mathrm{red}}=5\times10^6$, $D_d=0.05$, $D_u'=1$. (b) $h=0.21$, $a=0.29$, $m=0.024$, $c_0=0.003$, $k_1=4.2\times10^5$, $k_2=0.025578$, $k_3=3000$, $k_4=2.5578$, $k_7'=0.696$, $k_9=0.051m$, $k_{10}=0.05m$, $c_{\min}=1.07867\times10^{-5}$, $D_d=0.01$, $D_u'=1$.

Fig. 3(a). However, as we will see in our numerical simulations, the presence of Turing instability does not guarantee the emergence of Turing patterns in model (B). This feature probably arises from the large excitability of the SS in this system.

If the SS is close to the fully oxidized state ($z_{\mathrm{SS}}\cong c_0$), we also find wave instability, in some cases with negative dispersion, which can lead to inwardly propagating (anti)waves.[5] An example is shown in Fig. 3(b). Typically, models that produce a wave instability contain a second fast-diffusing activator (in addition to our activator x and inhibitor y). Here, we have no additional fast-diffusing activator. Instead, the same fast-diffusing inhibitor u that gives rise to Turing instability produces our wave instability, because the terms $2k_1xy$ and k_3x^2 that involve activator x are responsible for the production of u, thus coupling u with x.

B. Computer simulation of model (B)

To integrate the partial differential equations, we employ the commercially available software package FLEXPDE,[18] with a typical error (ERRLIM) of 1.0×10^{-7} for each variable in each spatial cell. Simulations were performed both in 1D and two dimensions (2D).

A typical set of JW in 1D is shown in Fig. 4. Figure 4(a) is a space-time plot, in which the saltatory manner of wave propagation is clearly visible. Since the range of parameters for JW is surprisingly broad, we can easily control the wave speed and the length of a single jump by changing our parameters, in particular m, a, h, and k_9. The last constant depends on the concentration of BrMA and strongly affects the behavior of model (B). For the parameters we used, model (B) exhibits excitability in zero dimensions, i.e., without diffusion terms, and Turing instability when diffusion terms are included.

To understand the origin of this jumping behavior, we followed the values of all the model variables. Figure 4(b) shows the spatial distribution of variables z (oxidized catalyst) and y (inhibitor) at several times in the vicinity of the third jump shown in Fig. 4(a). The first panel of Fig. 4(b) is a coarse scaling, while the next three panels show a finer resolution. We see that when a peak of z forms, two peaks of y begin to grow at its edges, thus preventing the z-peak from

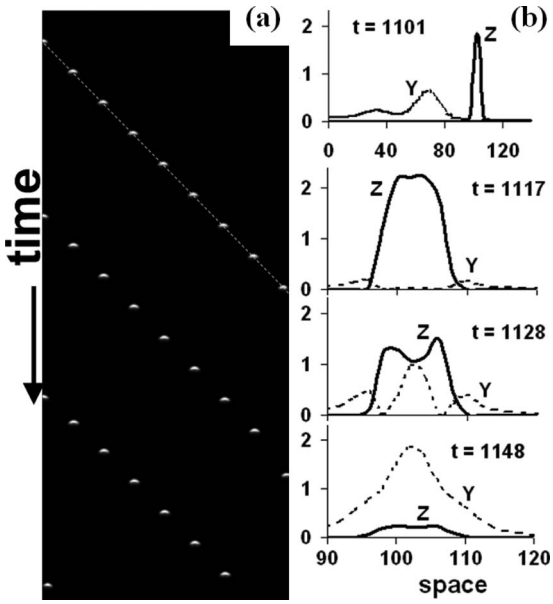

FIG. 4. (a) Space-time plot for JWs found in model (B) in 1D with zero-flux boundary conditions and a small perturbation of the SS at the left end. Total length is 280 a.u. for dimensionless diffusion coefficients $D_d=0.05$, $D_u'=1$ or 5.6 mm for dimensional coefficients $D_d=2\times10^{-7}$ and $D_u'=4\times10^{-6}$ cm^2/s. Total time =6000 s. White short segments correspond to high concentration of the oxidized catalyst z. Dotted line is drawn through the first wave. (b) Four concentration profiles of the catalyst z and inhibitor y. Space is in a.u.; concentrations are in milimolar. Parameters of model (B) are the same as in Fig. 3(a).

spreading. These y-peaks, and a third peak that emerges between them ($t=1128$), result from the fast diffusion of bromine (u). The z-peak is soon destroyed by the central y-peak, which grows in its place [two last panels of Fig. 4(b)]. The next z-peak arises in a distant region, where y and u are relatively small and x is relatively large (here, at position 135 a.u. and time 1428 s).

In Fig. 4(a), we see that after the first JW, a second wave emerges and then a third, despite the fact that the system is excitable (stable to small perturbations), not oscillatory. This behavior results from the proximity of the system to the onset of Hopf bifurcation: the initial perturbation decays via damped oscillations, which are large enough to induce a new cycle of excitability that starts at the left end of the segment. Therefore the frequency of JW, which is determined by that of the slowly decaying perturbation, is relatively small and there are no bulk oscillations in the system. We can change the parameters slightly, for example, by increasing h, and push the system into the oscillatory domain. An example of JW in this case (Hopf + Turing) is shown in Fig. 5. As in Fig. 4(a), we see JWs as cascading white dashes. In addition, the horizontal lines at the right represent bulk oscillations. The periods T_{JW} of JW and T_b of bulk oscillations are 1103 and 1317 s, respectively. The point at which the JW and bulk oscillation collide is a shock point. The velocity of this shock point (marked by the white dashed line) can be calculated from T_{JW}, T_b, L_J (the length of a single jump)$\cong$35 a.u. (cf. the Turing wavelength found from the dispersion curve as $2\pi/k_{\max}\cong15$ a.u.), and the time interval between two consecutive jumps $T_J=191$ s as $(T_b-T_{\mathrm{JW}})L_J/(T_JT_{\mathrm{JW}})$

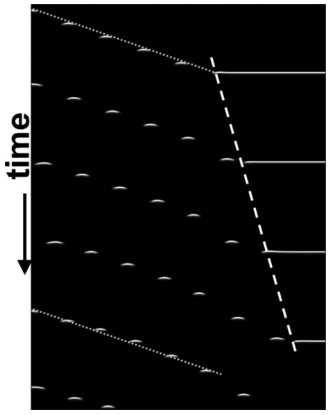

FIG. 5. Space-time plot for JWs in model (B) for 1D with zero-flux boundary conditions, small perturbation of the SS at the left end, and bulk oscillations (Hopf bifurcation). Parameters as in Fig. 4 except $h=0.11$. Size $=280$ a.u. $\times 6000$ s.

$=0.025$ a.u./s (cf. $L_J/T_J=0.183$ a.u./s). An analogous shock point was observed in the experiment.[8]

Since the range of parameters for JW is very broad and JW can arise when the system exhibits Turing instability, excitability and/or Hopf instability (bulk oscillations), it is important to determine whether such behaviors as Turing patterns and conventional continuously propagating waves can also occur in this model as they do in the actual BZ-AOT system. Turing patterns [Fig. 6(a)] are found at very small diffusion coefficient D_d for species x, y, and z. Note that the distance between the outer z-peaks is about $5.2\lambda_T$, where $\lambda_T=5.24$ is the Turing wavelength obtained from the dispersion curves by linear stability analysis, while the distance between the two central z-peaks is $\lambda_T/2$. These two central peaks emerge first due to a small, narrow initial perturbation at the middle of the segment, while the other peaks arise later as the perturbation spreads out from the central peaks. The problem of stabilization of large-amplitude and sharp Turing patterns is still an open question. We cannot predict their wavelengths. Only for small-amplitude Turing patterns (for which the concentrations are close to their SS values), can we guarantee that the observed Turing wavelength will be

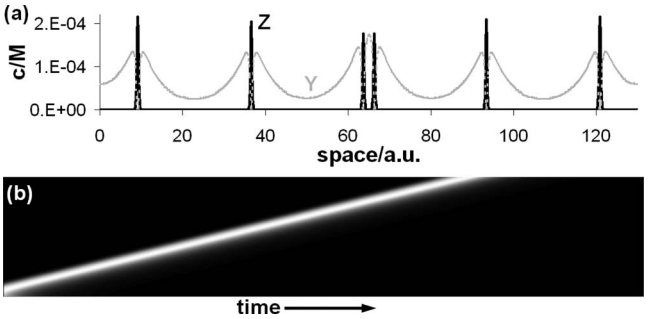

FIG. 6. (a) Turing pattern found in model (B) in 1D with zero-flux boundary conditions and small local perturbation of the SS at the center. Total length=130 a.u. Concentrations of z and y are in M. Parameters are the same as in Fig. 3(a) except $D_d=0.001$. (b) Space-time plot of a simple (continuous) traveling pulse in model (B) in 1D with zero-flux boundary conditions and small local perturbation of the SS at the left end of the segment. Size=180 s $\times$ 260 a.u. Parameters: $h=0.1$, $a=0.2$, $m=0.6$, $k_9=0.2m$, $k_7'=29m/150$, $D_X=2$, $D_Y=D_u'=1$, $D_Z=0.5$, other parameters as in Fig. 3(a).

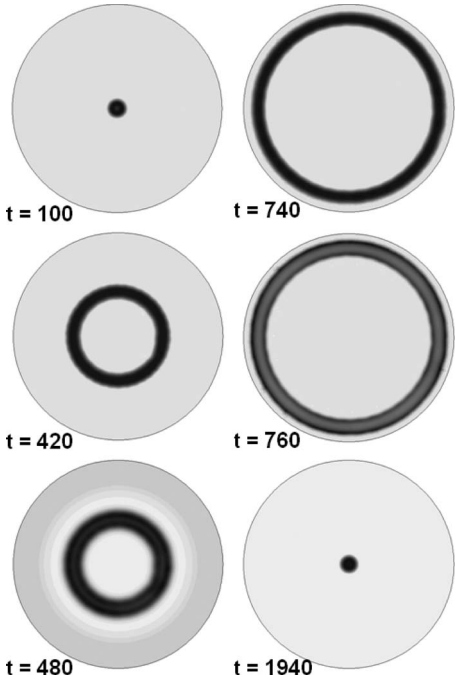

FIG. 7. Snapshots of JWs found in model (B) in 2D with a small perturbation at the center of a circle of radius 80; zero-flux boundary conditions, z-variable. Darker color indicates higher concentration of z. All parameters are the same as in Fig. 3(a).

near λ_T. Traveling waves [Fig. 6(b)] occur when species x, y, and z diffuse more rapidly. In these simulations, we used slightly different coefficients D_X, D_Y, and D_Z instead of a single D_d for all species.

The JW found in 1D can assume various shapes in 2D. In Fig. 7, we show circular JW found in 2D. In Fig. 8, we show bubble waves found at another set of parameters. In

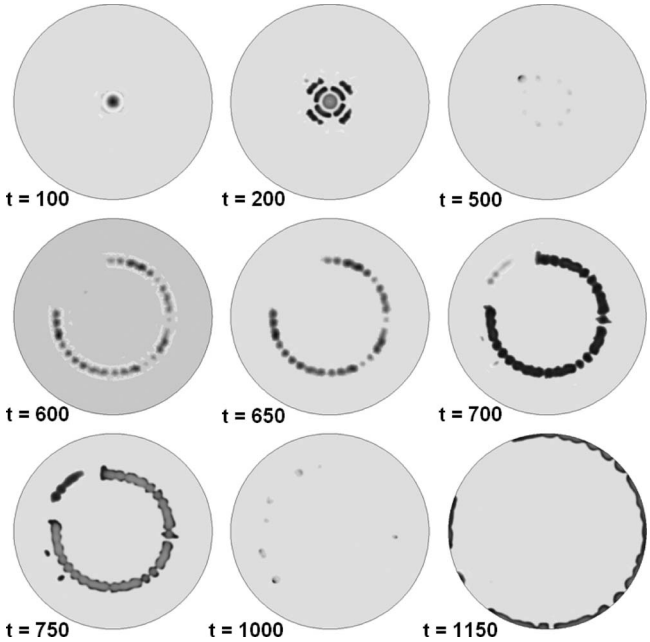

FIG. 8. Snapshots of bubble waves in model (B) in 2D with a small perturbation in the center of a circle of radius 30; zero-flux boundary condition, z-variable. Darker color indicates higher concentration of z. Parameters: $h=0.08$, $a=0.05$, $m=0.1$, $c_{\min}=2.856\,57\times10^{-5}$, $k_7'=0.725$, $D_X=D_Y=0.001$, $D_Z=0.0005$, $D_u'=1$, all other parameters as in Fig. 3(a).

1D, the waves found with these parameters resemble ordinary JW. In 2D, however, each emerging ring splits into many small circular waves that look like small bubbles. When bubbles collide, they annihilate. This splitting is due to a Turing instability of the smooth circular ring. Bubbles can move independently of one another. As a result, some bubbles propagate (by jumping) slightly faster or have slightly larger jump lengths (L_J) than others (upper left quadrants of snapshots in Fig. 8, where bubbles emerge at $t=700-750$, while in other areas, bubbles emerge at $t \cong 600$). In these simulations we made D_Z slightly smaller than $D_X = D_{Y'}$ though this condition is not essential for BW. The 2D simulations are quite time-consuming, and we did not investigate a broad range of parameters as we did in 1D.

IV. DISCUSSION

We have developed a new model for the BZ and BZ-AOT systems and found that this model is capable of simulating the JW and BW found in recent experiments.[8] The results suggest that JW and BW arise from a combination of Turing instability and excitability or Turing + Hopf, rather than from a wave instability as suggested previously.[8,19] That this model is derived from the detailed FKN mechanism and is able to explain BW, which could not be obtained with earlier models containing a wave instability, is encouraging. The existence of two different mechanisms that show JW emphasizes the fact that any single pattern in a reaction-diffusion system may have multiple explanations. To evaluate a proposed mechanism, one needs to see if it reproduces other patterns close in the parameter space to the pattern of interest. Further tests of model (B) might, for example, use it to simulate segmented waves.[20,21] Note that we have used in our present simulations the same constants employed in the FKN mechanism for the BZ reaction in the aqueous phase.

We anticipate that models (A) and (B) will find many applications, for example, in simulations of diffusively coupled BZ-droplets[9] or in investigating additional patterns in the BZ-AOT system,[22] where bromine is important as a messenger molecule.

ACKNOWLEDGMENTS

This work was supported by the National Science Foundation through Grant No. CHE-0615507.

[1] B. P. Belousov, *A Periodic Reaction and Its Mechanism* (Medgiz, Moscow, 1959), pp. 145–152.
[2] A. M. Zhabotinsky, Dokl. Akad. Nauk. USSR **157**, 392 (1964).
[3] R. J. Field, E. Körös, and R. M. Noyes, J. Am. Chem. Soc. **94**, 8649 (1972).
[4] R. J. Field and R. M. Noyes, J. Chem. Phys. **60**, 1877 (1974).
[5] V. K. Vanag and I. R. Epstein, Phys. Rev. Lett. **88**, 088303 (2002).
[6] A. Kaminaga, V. K. Vanag, and I. R. Epstein, Angew. Chem., Int. Ed. **45**, 3087 (2006).
[7] V. K. Vanag and I. R. Epstein, Phys. Rev. Lett. **92**, 128301 (2004).
[8] A. A. Cherkashin, V. K. Vanag, and I. R. Epstein, J. Chem. Phys. **128**, 204508 (2008).
[9] M. Toiya, V. K. Vanag, and I. R. Epstein, Angew. Chem., Int. Ed. **47**, 7753 (2008).
[10] S. Kádár, T. Amemiya, and K. Showalter, J. Phys. Chem. A **101**, 8200 (1997).
[11] V. K. Vanag, A. M. Zhabotinsky, and I. R. Epstein, J. Phys. Chem. A **104**, 8207 (2000).
[12] T. Amemiya, T. Ohmori, and T. Yamaguchi, J. Phys. Chem. A **104**, 336 (2000).
[13] A. L. Kawczynski, W. S. Comstock, and R. J. Field, Physica D **54**, 220 (1992).
[14] B. Peng, V. Gáspár, and K. Showalter, Philos. Trans. R. Soc. London, Ser. A **337**, 275 (1991).
[15] V. K. Vanag, Phys.-Usp. **47**, 923 (2004).
[16] L. Garcia-Rio, J. C. Mejuto, R. Ciri, I. B. Blagoeva, J. R. Leis, and M.-F. Ruasse, J. Phys. Chem. B **103**, 4997 (1999).
[17] V. K. Vanag and I. Hanazaki, J. Phys. Chem. **100**, 10609 (1996).
[18] FlexPDE (http://www.pdesolutions.com).
[19] L. F. Yang, A. M. Zhabotinsky, and I. R. Epstein, Phys. Chem. Chem. Phys. **8**, 4647 (2006).
[20] V. K. Vanag and I. R. Epstein, Phys. Rev. Lett. **90**, 098301 (2003).
[21] V. K. Vanag and I. R. Epstein, Proc. Natl. Acad. Sci. U.S.A. **100**, 14635 (2003).
[22] V. K. Vanag and I. R. Epstein, Phys. Rev. Lett. **87**, 228301 (2001).